Adv. Sci. Res., 12, 11–21, 2015
www.adv-sci-res.net/12/11/2015/
doi:10.5194/asr-12-11-2015

Advances in Science & Research
Open Access Proceedings

Wind variability in a coastal area (Alfacs Bay, Ebro River delta)

P. Cerralbo[1], M. Grifoll[1,2], J. Moré[3], M. Bravo[3], A. Sairouní Afif[3], and M. Espino[1,2]

[1]Maritime Engineering Laboratory, Polytechnic University of Catalonia (LIM/UPC), c./Escar, 6, 08039 Barcelona, Spain
[2]International Centre of Coastal Resources Research, Polytechnic University of Catalonia (CIIRC/UPC), c./Jordi Girona, 1–3, 08034 Barcelona, Spain
[3]Servei Meteorològic de Catalunya (SMC), c./Berlín, 38–46, 08029 Barcelona, Spain

Correspondence to: P. Cerralbo (pablo.cerralbo@upc.edu; pablocerralbo@gmail.com)

Received: 26 November 2014 – Revised: 28 January 2015 – Accepted: 16 February 2015 – Published: 3 March 2015

Abstract. Wind spatial heterogeneity in a coastal area (Alfacs Bay, northwestern Mediterranean Sea) is described using a set of observations and modelling results. Observations in three meteorological stations (during 2012–2013) along the coastline reveal that wind from the N–NW (strongest winds in the region) appears to be affected by the local orography promoting high wind variability on relatively short spatial scales (of the order of few kilometres). On the other hand, sea breezes in late spring and summer also show noticeable differences in both spatial distribution and duration. The importance of wind models' spatial resolution is also assessed, revealing that high resolution (= 3 km) substantially improves the results in comparison to coarse resolution (9 km). The highest-resolution model tested (400 m) also presents noticeable improvements during some events, showing spatial variability not revealed by coarser models. All these models are used to describe and understand the spatial variability of the typical wind events in the region. The results presented in this contribution should be considered on hydrodynamic, ecological and risk management investigations in coastal areas with complex orography.

1 Introduction

In the open sea and ocean, wind variability responds mostly to mesoscale structures like cyclones and anticyclones, as well as more permanent structures such as easterly (polar) and westerly (middle latitudes) winds. But when orographic constraints appear, such as oceanic islands (Chavanne et al., 2002) or mountains in coastal areas (Jiang et al., 2009), the wind presents high spatial variability, showing important curl gradients and becoming less predictable. In coastal areas, several examples of high spatial variability due to topographic constraints have been described (e.g. Herrera et al., 2005; Boldrin et al., 2009). In recent years, the application of numerical models in both the atmosphere and oceans has contributed to improving the understanding and description of this variability (Schaeffer et al., 2011). Moreover, modelling studies have revealed that the model resolution is a key factor for the correct representation of wind patterns, which could be essential in a correct prediction of flood episodes (Brecht and Frank, 2014) and could allow for the correct application of hydrodynamic modelling (Signell et al., 2005; Bignami et al., 2007). Several authors have described wind variability in lakes (e.g. Venäläinen et al., 2003), whilst only few studies focused on the wind description in a small-scale domain such as small estuaries or coastal areas. Considering the importance of wind on hydrodynamics, water mixing, waves and air quality, this contribution seeks to fulfill this gap, presenting an example of wind variability in a small-scale coastal area through observations and modelling results. A small bay, Alfacs Bay, in the northwestern Mediterranean Sea was selected.

This contribution is organized as follows. First, a short description of the study area (Sect. 2) and the set of observations is presented (Sect. 3). In this section the spatial and temporal variability observed is described. Then, the numeri-

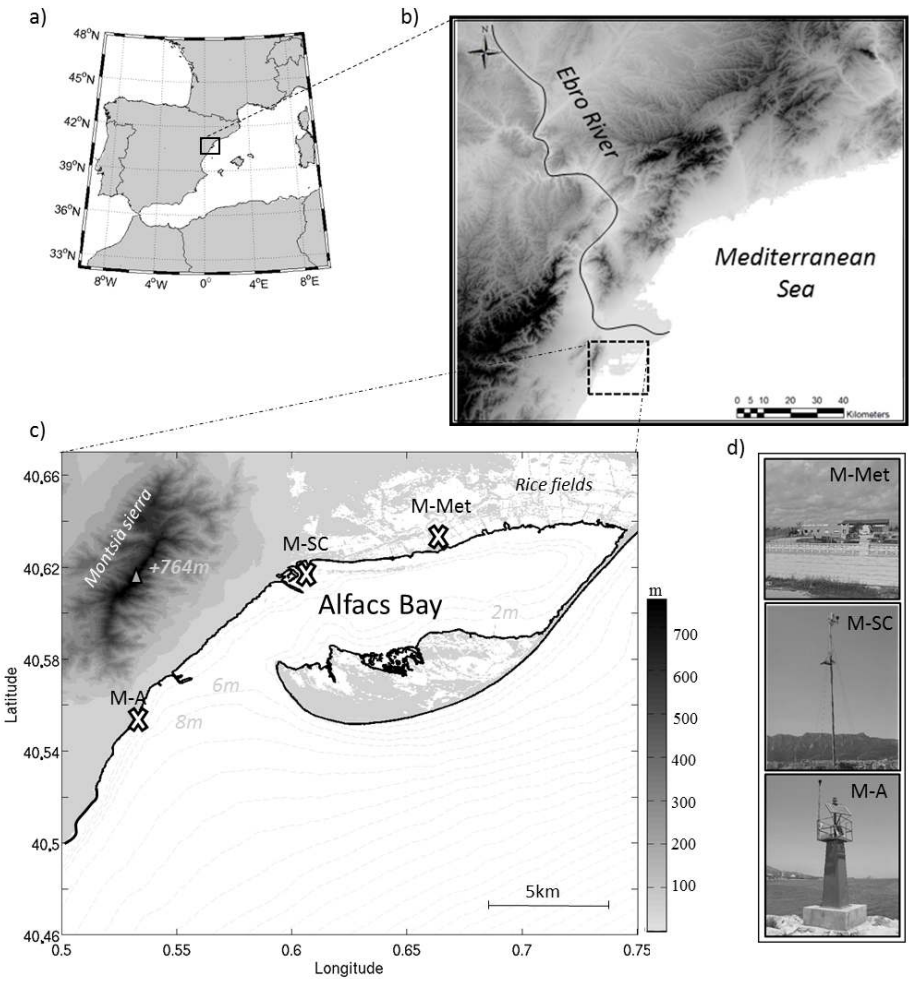

Figure 1. **(a)** Location map. **(b)** Ebro River delta region, with Alfacs Bay delimited by dashed square. **(c)** Study area showing meteorological stations (white crosses): M-A for Les cases d'Alcanar station, M-SC for Sant Carles de la Ràpita harbour station and M-Met for Meteocat station. Colour bar indicates altimetry above mean sea level. The bathymetry is also shown (isobaths, each 2 m). **(d)** Meteorological stations pictures.

cal weather prediction model implementation and outputs are shown, compared to the observed winds (Sect. 4). Finally, results for selected wind events and patterns observed are discussed.

2 Study area

The Ebro Delta (NE coast of Spain) forms two semi-enclosed bays, Fangar and Alfacs (to the north and south, respectively). The dimensions of Alfacs Bay are 16 km from head to mouth (Fig. 1c), 4 km wide and a mouth connection to the open sea of about 2.5 km. The bay is surrounded by rice fields to the north – which spill around 10 $m^3 s^{-1}$ of freshwater 10 months per year to the bay (Serra et al., 2007) – and a sand beach enclosing it on the eastern side, which can suffer breaching processes under severe storm conditions (Gracia et al., 2013). Serra de Montsià, with maximum altitudes around 700 m, closes the bay on the west side (Fig. 1).

The synoptic winds on the Catalan coast are affected by orographic constraints, such as the blocking winds of the Pyrenees that promote tramuntana (N) and mistral (NW) winds over some areas, and the wind channelling due to river valleys (Sánchez-Arcilla et al., 2008). Northerly winds in the region are mainly produced by high pressures over the Azores and lows over the British Isles and Italy; other synoptic situations could also lead to strong winds from the NW in the Ebro Delta (Martín Vide, 2005). Winds in the bay have been characterized as having a northwestern and southwestern predominance, with the strongest ones coming from the NW (channelized by the Ebro River valley; see Fig. 1b), being also the most common strongest winds on the Catalan coast during autumn and winter (Bolaños et al., 2009). On the other hand, some authors have reported the high spatial

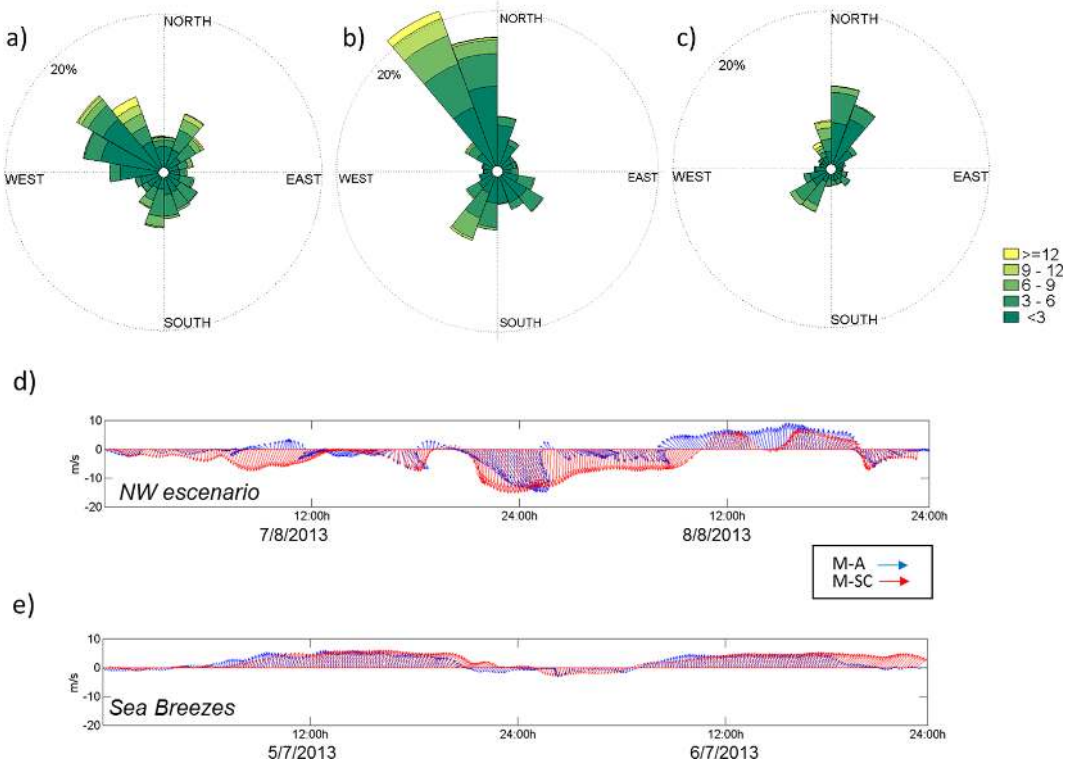

Figure 2. Wind roses for M-A **(a)**, M-Met **(b)** and M-SC **(c)** during the period 2012–2013. Velocities – colour bar in **(c)** – are in $\mathrm{m\,s^{-1}}$. Dotted line indicates frequency of 20 %. Wind time series for northwesterlies and sea breeze events in **(d)** and **(e)**, respectively. For **(d)** and **(e)**, a Lanczos filter of 2 h has been applied to the 10 min wind data.

heterogeneity of the wind fields inside the bay (Camp, 1994), in agreement with observed events during field campaigns by the authors of this manuscript, in which winds from the northwest were blowing inside the bay whilst in the mouth of the bay the wind was almost calm.

3 Observations

Atmospheric data – wind, atmospheric pressure, solar radiation and humidity – were obtained from three fixed land stations: Alcanar (M-A); Sant Carles (M-SC) from Xarxa d'Intruments Meteorològics de Catalunya (XIOM) described in Bolaños et al. (2009); and Alfacs-Meteocat (M-Met), which belongs to the automatic weather stations network of the Meteorological Service of Catalunya (http://www.meteocat.cat). Pictures of the stations are found in Fig. 1d. Both M-A and M-SC are at 10 m above the ground, while M-Met measures at 2 m. In order to compare wind intensities from all stations, we have adapted the measurements at 2m to the standard height of 10 m. The method adapted in Herrera et al. (2005) from Oke (1987) is used to compute the velocities at 10 m (w_{10}) from the observed values (w_h), following $w_{10} = w_h \frac{\log\left(\frac{10}{zs}\right)}{\log\left(\frac{h}{zs}\right)}$, where h represents the measurement height (2 m). Following Agterberg and Wieringa (1989), we have considered a typical roughness (z_s) for plains with low vegetation (rice fields) of ≈ 0.03 m. The roughness variability as a function of the wind direction is not considered.

Observations from June 2012 to June 2013 at three meteorological stations show noticeable differences (Fig. 2), confirming high variability among them. This period has been chosen for this analysis because it is the only one with data from all three stations. In M-SC (Fig. 2c) a bimodal behaviour with the most common winds from the southwest and north–northeast are shown. These winds are in agreement with data acquired at the same station for about 16 years (not shown), indicating high representation for the period selected. The highest intensities correspond to N–NW winds ($> 9\,\mathrm{m\,s^{-1}}$). For M-A the directions are more scattered, the most common winds being from W-NW to NW. The highest-intensity winds still come from the NW–NE, but the purely northern winds are less common. Finally, winds from M-Met show also a clear bimodal behaviour, with winds from the NW and SW–SE being the most common. However, M-Met is altered by the human buildings on the south side, which would alter on the wind measurements. Among the three stations most of the differences are clearly seen in land winds due to possible effects of the Serra de Montsià mountain range, showing high heterogeneity in wind fields in short distances. To better understand the wind variability, directional

Table 1. Summary of the main characteristics of the three different model configurations used in this study.

Model	Domain	Nominal resolution	Lead time	Outputs
WRF9	Iberian Peninsula	9 km	72 h	3 h
WRF3	NE Spain	3 km	48 h	1 h
CALMET	SW Catalonia	0.4 km	48 h	1 h

scatter plots for stations with data at 10m height are shown in Fig. 3a. The corresponding mean velocity for the two stations (M-A and M-SC) is also shown in colours. This figure shows that winds from the SW–SE in M-A are rotated 20–30° clockwise in M-SC, as well as that winds from the NW–N in M-A seem to be rotated a bit clockwise in M-SC (also seen in Fig. 2). On the other hand, winds from W to NW in M-SC are not observed as in M-A; M-SC concentrates more on the N–NE winds. All these data illustrate that Serra de Montsià (Fig. 1) could act as a physical barrier to some type of northerly winds, redirecting them. These effects are probably most clear on mistral winds (NW), which are not completely reproduced by M-SC (Fig. 2d) but oriented to the north. Another meteorological station was planned to be operating between these two stations, but in the end it was no possible to deploy it. The winds from the SW–SE correspond mainly to see breezes in spring and summer (Bolaños et al., 2009). The time and spatial evolution of sea breeze differences between stations are also observable (Fig. 2e). Weak nocturnal offshore winds (NW) rotate and increase in intensity until the maximum of around 5 m s^{-1} and S–SW direction in M-A is reached. Similar behaviour is observed in M-SC, but the nocturnal winds come from the NE and the rotation is very noticeable, as breezes arise in the afternoon from the SW. In M-Met the behaviour is almost the same as M-A. All these data reflect that even during sea breezes the orography and probably variation of land uses (rice fields in the delta's plain versus brush forest in Serra de Montsià) affect the direction, intensity and durability of winds. Winds from the S–SE (not related to sea breezes) are also probably affected by topography (Fig. 3), but there are not enough observations to investigate the spatial variability in this case. The lack of wind data just in front of Serra de Montsià does not allow us to know the exact behaviour of NW (mistral) winds and sea breezes in the mouth of the bay, but the use of numerical models would allow us to approximate the corresponding theoretical wind patterns. The wind module reveals good agreement between both stations (not shown). Thus indicating most of the variability related to direction. All the observations are based on 1-year-long data, so no climatic conclusion is expected from our analysis.

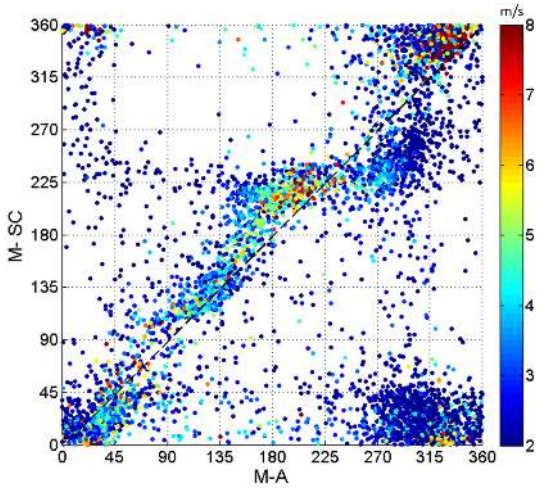

Figure 3. Wind direction comparison between M-A and M-SC for 1 year. The coloured data indicate mean wind velocity values (m s^{-1}) from both stations.

4 Numerical modelling

4.1 Description

Two different atmospheric models, provided by Meteocat, are used in this study to assess the role of spatial heterogeneity in the bay. For this purpose, the Weather Research and Forecasting (WRF) model has been selected (see http://www.wrf-model.org/), in particular the dynamical solver called Advanced Research WRF (WRF-ARW). The WRF-ARW is a model that has a worldwide community of users. It is a fully compressible, non-hydrostatic mesoscale model (Skamarock et al., 2008) and is based on solving the primitive equations of the atmosphere with different physical parameterizations available. Version 3.1.1 is used, with some minor code changes that consider an increase of the surface stress parameter (u-star) by a factor of 20 % in order to address the surface wind overestimation in the WRF model that has been reported by several authors (Mass and Ovens, 2011). By introducing this modification, a better agreement with meteorological observations is obtained. In later versions of the WRF model, more sophisticated corrections have been incorporated in the same direction, such as a surface drag parameterization scheme which allows enhancing the u-star depending on the sub-grid terrain variance (Mass and Ovens, 2011). The main parameterizations used are the Thompson scheme (Thompson et al., 2004) for microphysics, the YSU scheme (Hong et al., 2006) for planetary boundary layer and the unified Noah land surface model (Tewari et al., 2004) for surface physics. More configuration details are available at http://www.meteo.cat. This model is run using Global Forecast System (GFS) data as initial and boundary conditions (with 0.5° and 6 h spatial and temporal resolution). Two different configurations depending on grid resolution have been analysed: 9 and 3 km (named hereafter WRF9 and WRF3).

The main model parameters are summarized in Table 1. Not only spatial resolution is different between them; temporal resolution is also different. These configurations correspond to the available products of the Meteocat meteorological operational forecast system.

On the other hand, an additional simulation has been considered to derive atmospheric data at a very high resolution (400 m). In particular, the WRF-ARW outputs at 3 km are downscaled by a diagnostic meteorological model called CALMET. CALMET, a component of the CALPUFF Modeling System designed for the simulation of atmospheric pollution dispersion (Scire et al., 1999), is a diagnostic three-dimensional meteorological model which includes parameterized treatments of slope flows, kinematic terrain effects and terrain blocking effects, among others. These particular aspects help to better represent regional flows with an efficient computational cost.

The operational numerical model resolutions (spatial and temporal) were selected considering both reliability and computational costs. The computational cost for a 3-day forecast for CALMET (at 400 m resolution) is about 2 h using 10 CPUs. On the other hand, a similar domain and forecast horizon using WRF3 (3 km of resolution) take around 1 h (30 CPUs). In this sense, the application of WRF at higher resolution is not currently considered as an operational product due to computational limitations. For all the verification processes the daily first 24 h of prediction from the operational system are used.

4.2 Model verification

In this section, we present the results of verification studies to assess the performance of wind velocity and direction prediction from the models against the observation. The verification of both WRFs (WRF3 and WRF9) and CALMET is shown in Fig. 4 for summer 2013 (Fig. 4a) and winter 2014 (Fig. 4b). Different oceanographic campaigns were developed at Alfacs Bay during the same periods. We chose that period in order to coincide the meteorological observations and model results with oceanographic data. Verification of all the models and resolutions is done against hourly means from observational data. The wind module velocities measured in both M-A and M-SC are graphically compared to modelling results for both systems (model data is interpolated through bi-lineal interpolation to corresponding points) using a Taylor diagram (Taylor, 2001). In this diagram we can observe the comparison between observations and model through the correlation, the centred root-mean-square difference (CRMSD) and the standard deviations (SDs; see Appendix). In order to compare in the same figure different models against different observations, the standard deviations and CRMSD are normalized over the standard deviation of the corresponding observations (Grifoll et al., 2013). The model skill improves as the points get closer to the observation reference point in the diagram. In summer 2013, better correlation (around 0.6) is observed in M-SC, while in M-A the values decrease to ≈ 0.5. The standard deviation shows that the model presents lower-amplitude variations than the observed values. In spring 2014 only values from M-A were available. In this period, the correlations are higher for all models, and the SDs are more similar to the observations. Differences through different models are only observable in M-SC locations, revealing the highest correlations and lower errors in higher-resolution models (best results corresponding to CALMET). In M-A, the models do not show noticeable differences.

The wind module velocities measured in both M-A and M-SC are compared in Fig. 5a and b, respectively, for summer 2013 with modelling results using a Weibull distribution, which is defined as a two-parameter function commonly used to fit the wind speed frequency distribution. In both stations, the best fit between the model and observational Weibull distributions is observed for CALMET. In M-A, CALMET and the observational distribution show almost equally shaped coefficient; even observational data present stronger winds. WRF3 also has similar shape, with even more energy distributed at medium wind intensities ($= 3\,\mathrm{m\,s^{-1}}$). WRF9 seems to overestimate the mean winds. In M-SC, winds from CALMET are the most similar to observations, even overestimating the frequency of mean winds, and then not reproducing the maximum intensities (6–$10\,\mathrm{m\,s^{-1}}$). On the other hand, WRF3 and WRF9 overestimate both mean wind intensities and corresponding frequencies. In the winter season, observations show higher wind intensities, and both CALMET and WRF3 present Weibull shapes (not shown) similar to observations.

Some characteristic events representing the most usual winds in the area have also been analysed in order to understand the behaviour of each model under different conditions (resumed in Table 2). A period of 3 days is considered to have enough data to compare. Results show that winds from CALMET and WRF3 have higher correlations (except in northwest 2) than WRF9. The worst results are observed during northwesterly winds in summer 2013. This is clearly affected by the topography, and the observed wind in M-A is not reproduced by any of the models. Slightly better results are obtained in M-SC, especially by CALMET (but still with poor correlation). This event was characterized by its shortness (less than 6–8 h) and unsteadiness. On the other hand, in the winter period, another NW wind event (lasting for more than 1 day) was reproduced with noticeable agreement in M-A. In this case, the simulation WRF9 seems to reproduce quite well the wind time series in M-A, but no data for M-SC are available to compare. Southern winds – southeast and diurnal regime of sea breeze – are better reproduced by the finest models, being the highest improvement between WRF3 and WRF9. During sea breezes and considering the complete diurnal–nocturnal cycle, the CALMET model seems to reproduce winds better than the coarser ones. Considering the daily duration of the sea breeze – between 6 and 8 h – all the

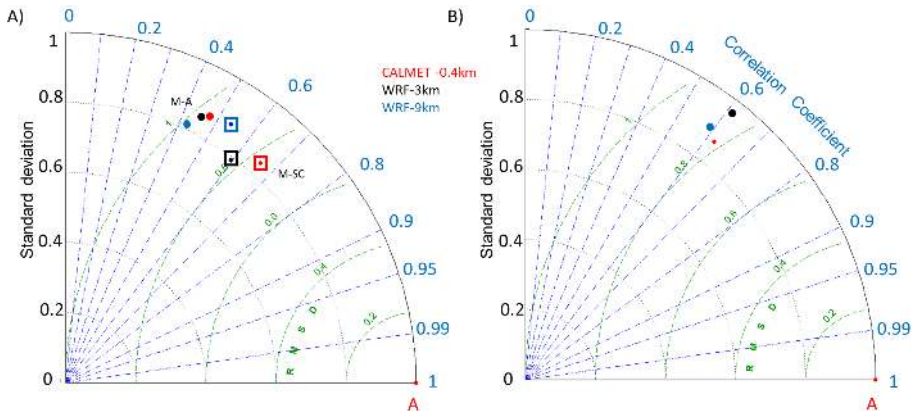

Figure 4. Taylor diagram for summer 2013 **(a)** and winter 2014 **(b)** for both M-A (coloured dot) and M-SC (coloured square filled with dot) model configurations (red for CALMET, black WRF3 and blue for WRF9) compared to corresponding meteorological stations. Both modelled standard deviations and RMSD are normalized over observational standard deviation.

Table 2. Correlation among the three different atmospheric models and observational data for 3-day-long events during summer 2013 and winter 2014. No correlation for winter 2014 (M-SC dismantled on September 2013).

	Day	M-A			M-SC		
		WRF9	WRF3	CALMET	WRF9	WRF3	CALMET
Northwest	8 Aug 2013	.02	.01	.12	.21	.40	.46
Northwest 2	4 Apr 2014	.80	.72	.75	–	–	–
Southeast	13 Aug 2013	.43	.64	.64	.58	.71	.75
Sea breezes	6 Jul 2013	.64	.67	.74	.64	.66	.76
Northeast	28 Mar 2014	.75	.86	.83	–	–	–

models would be able to reproduce it (Table 2). However, the temporal variability of such processes could only be reproduced using high-temporal-resolution models (≈ 1 h).

4.3 Spatial patterns and wind variability

Model wind snapshots for the three different resolutions are used to understand the spatial structures associated with most common winds in the area (Fig. 6). Three events have been chosen, representing a case with higher variability (Fig. 6a, d and g) to one with an almost homogeneous wind field (Fig. 6c, f and i). For northwesterly winds (left column panels in Fig. 6) it is clear that Serra de Montsià exerts a physical barrier on wind fields, thus revealing areas in the inner bay with high wind intensities and areas down the mountain with almost calm winds or with different direction – shadow effect, described in other environments such as the Hawaiian Islands in Chavanne et al. (2002). These effects were also observed for winds coming from the north (not shown). Atmospheric pressure at surface on 4 April 2014 shows low pressure over the North Atlantic and a high-pressure area over north Africa. This synoptic situation promotes winds from the north–northwest (triggered by the Ebro River valley) in the study area. The modelled winds corresponding to observations in M-A and M-SC locations are similar, not showing all the direction variability measured in observations (Figs. 2 and 3). However, the wind patterns in both WRF3 and CALMET are similar and show spatial wind variability inside the bay, thus indicating that the medium-resolution model is able to reproduce topographic constraints under these circumstances. On the other hand, the coarser model (Fig. 6a) does not reveal such a variability – expected for the dimensions of the bay and model resolution, with pixels almost half of the bay size. In summary, CALMET reproduces with higher accuracy these kind of winds in M-SC, while in M-A the errors are similar to coarser models. Both stations are located near the maximum transition zone between high- and lower-intensity winds (Fig. 6g), corresponding to the areas where modelling errors would be more sensitive to topographic effects.

An intensification of sea breezes (Fig. 6b, e and h) at midday in inner areas of the bay is clearly represented as well as a clockwise gyre of wind in M-SC related to M-A. The modelled highest intensities in the inner bay are not able to be validated, due to the lack of more observational data in this area (M-Met has been defined as a bad indicator of wind field). On the other hand, differences from coarser to the finest model configurations are noticeable. Both WRF3 and CALMET show some spatial structures in daily regimes

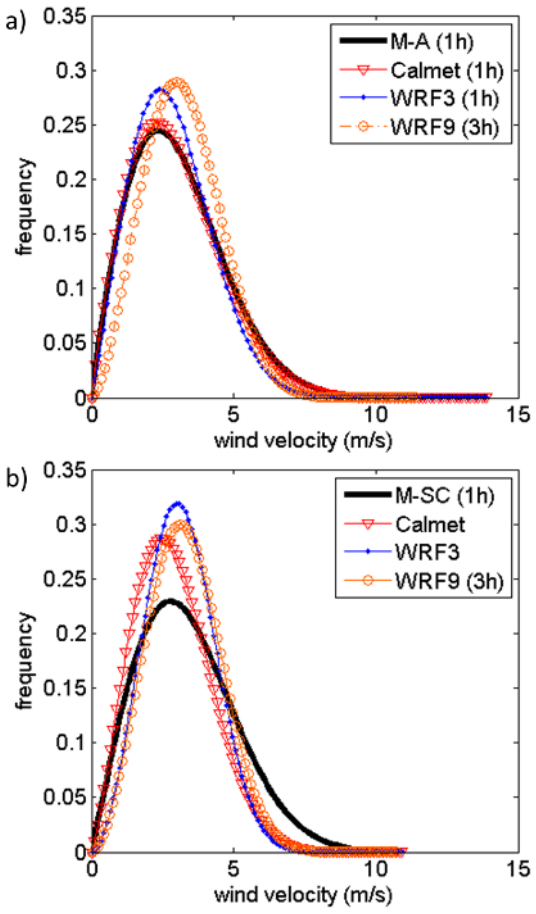

Figure 5. Weibull distributions for summer 2013 in M-A **(a)** and M-SC **(b)**. Black line for observational data (hourly) and coloured lines for each model configurations (red for CALMET, blue for WRF3 and orange for WRF9).

not solved by WRF9. In the time series, sea breezes time-lag between M-A and M-SC observations is not reproduced by any of the models.

On the other hand, spatially homogeneous wind fields have also been observed during several events. In this case, winds from the northeast are shown in Fig. 6c, f and i. The wind fields reproduced by observations and atmospherical models indicate homogeneous spatial winds, not affected by topography in the Ebro Delta (winds coming along the coast). For these winds, the coarser model does reproduce the wind pattern similar to the finest model. In Fig. 3a there is an area where directions around 0–45° shows high correlation between M-SC and M-A. However, in Table 2 the NE case shows that CALMET and WRF3 have better correlation than WRF9, indicating that in some cases the temporal resolution would also play an important role in wind prediction.

5 Final remarks

This contribution presents an example of high wind variability in a coastal area (Alfacs Bay, NW Mediterranean Sea) during the period 2012–2013. Observational data demonstrate that wind direction seems to be affected by the surrounding mountains. These effects are maximized during northwesterly winds, in which the local mountains exert noticeable shadowing effects over the mouth of the bay. These results are in agreement with Camp (1994), showing high wind spatial variability at Alfacs Bay, as well as other similar studies which show the wind-channelling effects in some rias of Galicia (Herrera et al., 2005). Other winds, like sea breezes, also show noticeable variability, not only in space but also in time, and probably related to orography, land uses and different sea-water temperature in the bay and in the open sea. Winds from the S–SE not related to sea breezes are likely affected by local orography, but not enough events were recorded to confirm the observed pattern. Due to the short length of observational period (around 1 year), the results have no climatic significance.

The spatial heterogeneity also plays an important role in wind modelling results in this coastal area. The coarse model (9 km) does not reproduce the spatial variability associated with most topographically influenced winds (northwesterlies and sea breezes). The medium-resolution model (3 km) has proven to represent the wind spatial fields with enough accuracy according to the observations. This indicates that the effects of the main topographic structures on the area are recognized by this resolution model, contrary to other places where similar model resolution was not able to reproduce all the wind variability due to orography (Cerralbo et al., 2012). The predicted wind from the CALMET model at the highest resolution (400 m) also improves the spatial variability and shows the highest correlation with observational data under some circumstances. In this sense, the CALMET model could be an interesting and useful product for ocean and wave modelling, minimizing the information losses due to the downscaling processes. In summary, all the systems analysed reproduce with enough accuracy some of the characteristic winds observed at Alfacs Bay. The highest-resolution model shows better responses, since it reproduces more realistically wind fields and discriminates topographic structures such as mountains and gaps between them. However, correlation in some cases is higher in coarse models (WRF9), agreeing with Signell et al. (2005), who demonstrate that sometimes the higher-resolution models would present lower correlation due to higher "noise" (more variability) compared to the coarser models. Other authors (e.g. Miglietta et al., 2012; De Biasio et al., 2014) also argue that local models could show more details (more detailed flow patterns) although worse statistics due to errors in timing and location, whilst global models would produce smoother results and probably much skillful forecasts. At this point, the computational cost

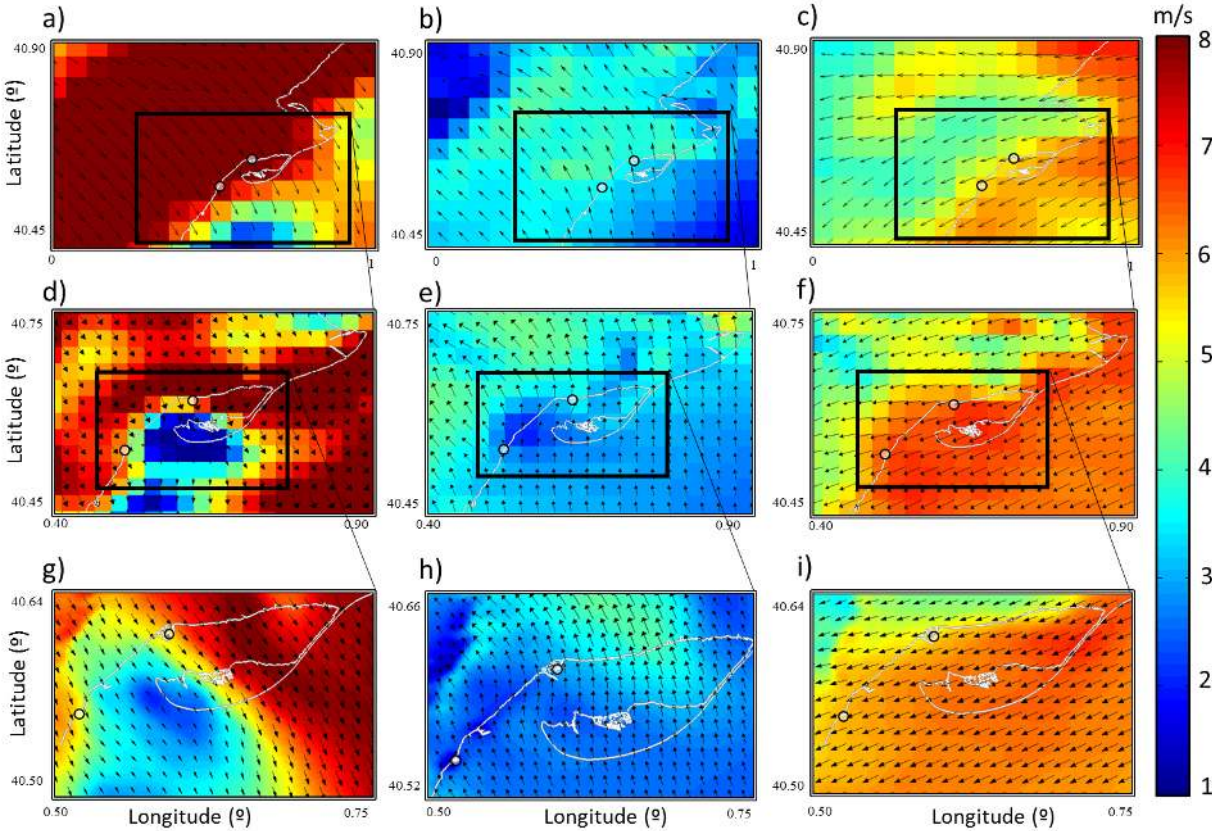

Figure 6. The three different models configurations are plotted for three snapshots of typical wind events at Alfacs Bay. **(a–c)** for WRF9 km, **(d–f)** for WRF3 and **(g–i)** for CALMET 400 m. Events represent winds from the northwest (left column panels) on 4 April 2014, sea breezes (central panels) on 6 July 2013 and northeasterly winds (right panels) on 12 March 2014. White circles indicate meteorological station locations (M-A and M-SC).

would indicate which should be the atmospheric model to be considered depending on the skill assessment requirements.

The effects of wind spatial variability on relatively short length scales would be an important factor to be considered in studies dealing with biology and ecology hazards, e.g. harmful algal blooms as described in Quijano-Scheggia et al. (2008), hydrodynamics (Cucco and Umgiesser, 2006) and water quality parameters (Grifoll et al., 2011) in coastal waters.

Appendix A: Statistics

The statistics used in the normalized Taylor diagram are defined as follows, where "obs" corresponds to observations, m corresponds to model results and the over bar (–) denotes all data length mean values:

$$\mathrm{SD} = \frac{\left(\sqrt{\frac{\sum_{i=1}^{n}(m_i - \overline{m})}{n}}\right)}{\mathrm{SD}_{\mathrm{obs}}}, \tag{A1}$$

$$\mathrm{CRMSE}(\mathrm{obs}, m) = \frac{\sqrt{\frac{\sum_{i=1}^{n}\left[\left(\mathrm{obs}_i - \overline{obs}\right) - \left(m_i - \overline{m}\right)\right]^2}{n}}}{\mathrm{SD}_{\mathrm{obs}}}, \tag{A2}$$

$$\mathrm{Correlation}(\mathrm{obs}, m) = \frac{\sum_{i=1}^{n}(m_i - \overline{m}) \cdot \left(\mathrm{obs}_i - \overline{\mathrm{obs}}\right)}{n \cdot \mathrm{SD}_{\mathrm{obs}} \cdot \mathrm{SD}_m}. \tag{A3}$$

Acknowledgements. This work was supported by a FPI-UPC pre-doctoral fellowship from the European project FIELD_AC (FP7-SPACE-2009-1-242284 FIELD_AC), the Spanish project PLAN_WAVE (CTM2013-45141-R) and the Secretariat d'Universitats i Recerca del Dpt. d'Economia i Coneixement de la Generalitat de Catalunya (Ref 2014SGR1253). The campaigns were carried out thanks to the MESTRAL project (CTM2011-30489-C02-01). We would like to thank Joan Puigdefàbregas, Jordi Cateura, Joaquim Sospedra and Elena Pallarés from Laboratori d'Enginyeria Marítima for all their help with campaigns and data analysis, as well as the Ebro Irrigation Community (Comunitat de Regants de la dreta de l'Ebre, http://www.comunitatregants.org) and the XIOM network (Xarxa d'Instruments Oceanogràfics de Catalunya; http://www.xiom.cat) for the information and their commitment to the study. Finally, we thank the two anonymous reviewers for their in-depth criticisms and suggestions.

Edited by: M. M. Miglietta
Reviewed by: two anonymous referees

References

Agterberg, R. and Wieringa, J.: Mesoscale terrain roughness mapping of the Netherlands, Technical Report TR-115, Royal Netherlands Meteorological Institute, Ministerie van Verkeer en Waterstaat, 1989.

Bignami, F., Sciarra, R., Carniel, S., and Santoleri, R.: Variability of Adriatic Sea coastal turbid waters from SeaWiFS imagery, J. Geophys. Res., 112, C03S10, doi:10.1029/2006JC003518, 2007

Bolaños, R., Jorda, G., Cateura, J., Lopez, J., Puigdefabregas, J., Gomez, J., and Espino, M. The XIOM: 20 years of a regional coastal observatory in the Spanish Catalan coast, J. Mar. Syst., 77, 237–260, doi:10.1016/j.jmarsys.2007.12.018, 2009.

Boldrin, A., Carniel, S., Giani, M., Marini, M., Bernardi Aubry, F., Campanelli, A., Grilli, F., and Russo, A.: Effects of bora wind on physical and biogeochemical properties of stratified waters in the northern Adriatic, J. Geophys. Res., 114, C08S92, doi:10.1029/2008JC004837, 2009.

Brecht, B. and Frank, H.: High resolution modelling of wind fields for optimization of empirical storm flood predictions, Adv. Sci. Res., 11, 1–6, doi:10.5194/asr-11-1-2014, 2014.

Camp, J.: Aproximaciones a la dinamica estuarica de una bahia micromareal Mediterranea, Thesis, Universitat de Barcelona, Barcelona, 1994.

Cerralbo, P., Grifoll, M., Espino, M., and López, J.: Predictability of currents on a mesotidal estuary (Ria de Vigo, NW Iberia), Ocean Dynam., 63, 131–141, doi:10.1007/s10236-012-0586-9, 2012.

Chavanne, C., Flament, P., Lumpkin, R., Dousset, B., and Bentamy, A.: Scatterometer observations of wind variations induced by oceanic islands: Implications for wind-driven ocean circulation, Can. J. Remote Sens., 28, 466–474, doi:10.5589/m02-047, 2002.

Cucco, A. and Umgiesser, G.: Modeling the Venice Lagoon residence time, Ecol. Model., 193, 34–51, doi:10.1016/j.ecolmodel.2005.07.043, 2006.

De Biasio, F., Miglietta, M. M., Zecchetto, S., and della Valle, A.: Numerical models sea surface wind compared to scatterometer observations for a single Bora event in the Adriatic Sea, Adv. Sci. Res., 11, 41–48, doi:10.5194/asr-11-41-2014, 2014.

Gracia, V., García, M., Grifoll, M., and Sánchez Arcilla, A.: Breaching of a barrier under extreme events, The role of morphodynamic simulations, J. Coast. Res., 951–956, doi:10.2112/SI65-161.1, 2013.

Grifoll, M., Del Campo, A., Espino, M., Mader, J., González, M., and Borja, A.: Water renewal and risk assessment of water pollution in semi-enclosed domains: Application to Bilbao Harbour (Bay of Biscay), J. Mar. Syst., 109–110, S241–S251, doi:10.1016/j.jmarsys.2011.07.010, 2011.

Grifoll, M., Aretxabaleta, A. L., Pelegrí, J. L., Espino, M., Warner, J. C., and Sánchez-Arcilla, A.: Seasonal circulation over the Catalan inner-shelf (northwest Mediterranean Sea), J. Geophys. Res.-Oceans, 118, 5844–5857, doi:10.1002/jgrc.20403, 2013.

Herrera, J. L., Piedracoba, S., Varela, R. A., and Rosón, G.: Spatial analysis of the wind field on the western coast of Galicia (NW Spain) from in situ measurements, Cont. Shelf Res., 25, 1728–1748, doi:10.1016/j.csr.2005.06.001, 2005.

Hong, S.-Y., Noh, Y., and Dudhia, J.: A new vertical diffusion package with an explicit treatment of entrainment processes, Mon. Weather Rev., 134, 2318–2341, doi:10.1175/MWR3199.1, 2006.

Jiang, H., Farrar, J. T., Beardsley, R. C., Chen, R., and Chen, C.: Zonal surface wind jets across the Red Sea due to mountain gap forcing along both sides of the Red Sea, Geophys. Res. Lett., 36, L19605, doi:10.1029/2009GL040008, 2009.

Martín Vide, J.: Los mapas del tiempo, Volumen 1 de Colección Geoambiente XXI. Davinci Continental, Editorial Davinci, Mataró, Barcelona, 219 pp., 2005.

Mass, C. F. and Ovens, D.: Fixing WRF's high speed wind bias: a new subgrid scale drag parameterization and the role of detailed verification, in: 24th Conference on Weather and Forecasting and 20th Conference on Numerical Weather Prediction, Preprints, 91st American Meteorological Society Annual Meeting, 23–27 January 2011, Seattle, WA, 2011.

Miglietta, M. M., Thunis, P., Pederzoli, A., Georgieva, E., Bessagnet, B., Terrenoire, E., and Colette, A.: Evaluation ofWRFmodel performances in different European regions with the DELTA-FAIRMODE evaluation tool, Int. J. Environ. Pollut., 50, 83–97, 2012.

Oke, T. R.: Boundary Layer Climates, 2nd Edn., Routledge, London, 1987.

Quijano-Scheggia, S., Garcés, E., Flo, E., Fernandez-Tejedor, M., Diogene, J., and Camp, J.: Bloom dynamics of the genus Pseudo-nitzschia (Bacillariophyceae) in two coastal bays (NW Mediterranean Sea), Scientia Marina, 72, 577–590, 2008.

Sánchez-Arcilla, A., González-Marco, D., and Bolaños, R.: A review of wave climate and prediction along the Spanish Mediterranean coast, Nat. Hazards Earth Syst. Sci., 8, 1217–1228, doi:10.5194/nhess-8-1217-2008, 2008.

Schaeffer, A., Garreau, P., Molcard, A., Fraunié, P., and Seity, Y.: Influence of high-resolution wind forcing on hydrodynamic modeling of the Gulf of Lions, Ocean Dynam., 61, 1823–1844, doi:10.1007/s10236-011-0442-3, 2008.

Scire, J. S., Robe, F. R., Fernau, M. E., and Yamartino, J.: A User's Guide for the CALMET Meteorological Model (Version 5.0), Earth Tech, Concord, MA, 1999.

Serra, P., More, G., and Pons, X.: Monitoring winter flooding of rice fields on the coastal wetland of Ebre delta with multitemporal remote sensing images, IEEE International Geo-

science and Remote Sensing Symposium, Barcelona, 2495–2498, doi:10.1109/IGARSS.2007.4423350, 2007.

Signell, R. P., Carniel, S., Cavaleri, L., Chiggiato, J., Doyle, J. D., Pullen, J., and Sclavo, M.: Assessment of wind quality for oceanographic modelling in semi-enclosed basins, J. Mar. Syst., 53, 217–233, doi:10.1016/j.jmarsys.2004.03.006, 2005.

Skamarock, W. C., Klemp, J. B., Dudhia, J., Gill, D. O., Barker, D. M., Duda, M., Huang, X.-Y., Wang, W., and Powers, J. G.: A description of the advanced research WRF version 3, NCAR Tech. Note NCAR/TN-475+STR, Nat. Cent. for Atmos. Res., Boulder, Colorado, 2008.

Taylor, K. E.: Summarizing multiple aspects of model performance in a single diagram, J. Geophys. Res., 106, 7183–7192, 2001.

Tewari, M., Chen, F., Wang, W., Dudhia, J., LeMone, M. A., Mitchell, K., Ek, M., Gayno, G., Wegiel, J., and Cuenca, R. H.: Implementation and verification of the unified NOAH land surface model in the WRF model, in: 20th conference on weather analysis and forecasting/16th conference on numerical weather prediction, American Meteorological Society, Seattle, WA, 11–15, 2004.

Thompson, G., Rasmussen, R. M., and Manning, K.: Explicit forecasts of winter precipitation using an improved bulk microphysics scheme, Part I: Description and sensitivity analysis, Mon. Weather Rev., 132, 519–542, 2004.

Venäläinen, A., Sahlgren, V., Podsechin, V., and Huttula, T.: Small-scale variability of the wind field over a typical Scandinavian lake, Boreal Environ. Res., 8, 71–81, 2003.